ELSEVIER

Contents lists available at ScienceDirect

Biomaterials

journal homepage: www.elsevier.com/locate/biomaterials



3D printed HUVECs/MSCs cocultures impact cellular interactions and angiogenesis depending on cell-cell distance



Charlotte Piard^{a,c}, Anjana Jeyaram^a, Yi Liu^a, John Caccamese^b, Steven M. Jay^a, Yu Chen^a, John Fisher^{a,c},*

- ^a Fischell Department of Bioengineering, University of Maryland, 3121 A. James Clark Hall, College Park, MD, 20742, United States
- b Department of Oral and Maxillofacial Surgery, University of Maryland School of Dentistry, University of Maryland Medical Center, R Adams Cowley Shock Trauma Center, Baltimore, MD, United States
- c Center for Engineering Complex Tissues, University of Maryland, 3121 A. James Clark Hall, College Park, MD, 20742, United States

ARTICLE INFO

Keywords: 3D printing Angiogenesis Paracrine signaling Bone tissue engineering EVs

ABSTRACT

Vascularization is a crucial process during the growth and development of bone 1, yet it remains one of the main challenges in the reconstruction of large bone defects. The use of in vitro coculture of human umbilical vein endothelial cells (HUVECs) and human mesenchymal stem cells (hMSCs) has been one of the most explored options. Both cell types secrete specific growth factors that are mutually beneficial, and studies suggested that cell-cell communication and paracrine secretion could be affected by a number of factors. However, little is known about the effect of cell patterning and the distance between cell populations on their crosstalk. In the present study, we showed that the separation and distance between ECs and MSCs populations affects angiogenesis by modulating cell-cell communication. HUVECs grown farther apart from MSCs (>400 µm) presented characteristics of an early stage of angiogenesis (migration/proliferation). Results showed an increase in the upregulation of VEGF, FGF-2, and ITGA3 (integrins) but a smaller fold change in the expression of VE-Cadherin and Ang-1. HUVECs were also still highly proliferative. On the contrary, HUVECs incubated closer (≤200 µm) to MSCs, showed signs of stabilization, mainly an increase in Ang-1 and VE-cadherin expression, as well as tighter monolayers. Conditioned media collected from HUVECs and MSCs grown ≤ 200 µm apart preferentially promoted tube formation, a later stage of angiogenesis, due in part to a significant increase in Ang-1 paracrine secretion. In addition, in groups in which fibers were printed farther apart (400 µm), cells produced EVs with a significantly increase cargo. Finally, in vivo experiment results showed an increase in blood vessels density and new bone thickness after 12 weeks of implantation in rat cranial defect, further suggesting the higher efficiency of indirect ECs/MSCs contact in prompting the release of paracrine signals that stimulate the angiogenesis of local tissues, and enhanced subsequent bone regeneration.

1. Introduction

Vascularization is a crucial process during the growth and development of bone [1], yet it remains one of the main challenges in the reconstruction of large bone defects. Technologies to control and direct neovascularization within a mineralized construct have been developed to improve clinical outcomes from bone grafting procedures. Many investigators have successfully demonstrated the use of different strategies to develop vascular structures, including growth factor delivery [2], channeled scaffolds [3], perfusion bioreactors [4], cell coculture [5], and cell functionalization [6]. The use of in vitro coculture of human umbilical vein endothelial cells (HUVECs) and human

mesenchymal stem cells (hMSCs) has been one of the most explored options, as it allows for concurrent creation of a vascular network as well as the target tissue [7–9]. It is well established that both cell types secrete specific growth factors that are mutually beneficial. For example, endothelial cells are known to secrete growth factors such as insulin growth factor-1 [10], endothelin-1, and bone-morphogenic protein-2, promoting osteogenic growth and differentiation of the MSCs [11].

Recently, studies suggested that cell-cell communication and paracrine secretion can be affected by the substrate microarchitecture [12], mechanical environment [13] or the matrix stiffness [14]. However, little is known about the effect of cell patterning and the distance

^{*} Corresponding author. Fischell Family Distinguished Professor & Department Chair, Fischell Department of Bioengineering, University of Maryland, 4102A Clark Hall, 8278 Paint Branch Drive, College Park, MD, 20742, United States.

E-mail address: jpfisher@umd.edu (J. Fisher).

between cell populations on their crosstalk. The precisely regulated architecture of different tissue types, such as osteons in bones, indicates that characteristic features related to the number, types, and spacing of cells might be critical to tissue function. We previously demonstrated that an osteon-like scaffold, with specific patterning of HUVECs and MSCs, improved neovascularization of the implant in vivo [15].

Until recently, recapitulating complex hierarchical structures in vitro has proved difficult due to limited manufacturing techniques, particularly while using biological materials. 3D printing (3DP) using a three-axis dispensing system, which builds 3D constructs by extruding fibers of cell-laden materials in a layer-by-layer fashion, offers a unique opportunity in tissue engineering, by enabling precise positioning of cells and biomaterials, tunable mechanical properties, fine control of the external and internal architecture [16]. Controlling those specific parameters can modulate cellular effects. For example, pore sizes of at least 300 µm have been shown to enhance bone formation and vascularization [17]. Could 3D printing also be used to improve angiogenesis by modulating the crosstalk between EC and MSCs, through the precise control of the distance between fibers?

In the present study, the overall objective was to investigate how the distance between 3D printed fibers (i.e. separation and distance between ECs and MSCs populations) affects angiogenesis by modulating cell-cell communication in different 3D printed co-cultures. For this reason, this paper mainly focused on the impact that cell distance and separation had on endothelial cells biology and functions, and their interactions. ECs and MSCs can communicate through three major mechanisms: (i) the direct interaction between membrane molecules of the two adjacent cells (tight junctions, adherent junctions), the secretion of (ii) diffusible factors that diffuse freely in the extracellular environment and interact with the target cells through specific receptors, and (iii) the release of extracellular vesicles (EVs). To this end, we separately analyzed ECs grown in different co-culture conditions, the paracrine secretions and the released EVs in the conditioned media. We then used functional assays to study the cells and conditioned media's angiogenic potential. In vitro angiogenesis assays provide a valuable tool for assessing the effect of angiogenic products as they enable the analysis of isolated processes that contribute to angiogenesis, such as ECs migration, proliferation, sprouting, branching, and lumen formation [18]. Finally, based on our in vitro results, we investigated whether optimized concentric 3D printed cocultures, with optimal spacing between cell populations, could support proper neovascularization in an in vivo model, and consequently osteogenic differentiation and bone regeneration.

2. Materials and methods

2.1. Cell culture

As described elsewhere [15], hMSCs (RoosterBio, Frederick, MD) were cultured in RoosterBasal Media supplemented with RoosterBooster, as per the manufacturer's specifications. Cells at passage P3 were used for the experiments. HUVECs (Lonza) were cultured in EBM-2 Basal Medium (Lonza) supplemented by EGM-2 SingleQuot Kit. Cells at passage P4 were used for the experiments. Rat primary aortic endothelial cells (RAECs) were purchased from Cell Biologics (Chicago, IL) and cultured according to manufacturer instructions. Rat MSCs (rMSCs) were purchased from RD Systems (Minneapolis, MN) and cultured in osteogenic media for 7 days prior to implantation. The osteogenic media contained growth media supplemented with 100 nM dexamethasone (Sigma, St. Louis, MO), 10 mM β -glycerophosphate (Sigma), and 173 mM ascorbic acid (Sigma). Cells at passage P4 were used for the experiments.

2.2. 3D printed cocultures preparation

All samples, for the six experimental groups, were 3D printed using

a commercial 3D printing system (3D Bioplotter, EnvisionTEC, Gladbeck, Germany). All printing supplies (30 cc barrel and 200 μm precision tips) were purchased from Nordson EFD (RI, USA). All 3D printed samples were about 1 mm in thickness and 8 mm in diameter and were comprised of concentric fibers (200 μm) separated from each other by a distance of either 0, 200 μm or 400 μm (Fig. 1). A circular design was chosen to mimic cortical bones, and more specifically osteons, or concentrical lamellae of bone matrix with in its center, the Haversian canal containing blood vessels. This design was also chosen for its geometric symmetry, with a simple radial consideration.

Type A porcine gelatin (300 g Bloom), fibrinogen and thrombin from bovine plasma were purchased from Sigma. The bioink was prepared by mixing 10w/v% fibrinogen and 5w/v% gelatin and heating to $60\,^{\circ}\text{C}$ for $15\,\text{min}$. Cells were then passaged, suspended in media and centrifuged to form a pellet. After aspiration of the supernatant, the pellet was then suspended in the fibrin bioink by manual pipetting, until the solution was homogenous and all clumps were broken down. Three fibrin bioink formulations were prepared using: (1) HUVECs at a density of $2\times106\,\text{cells/mL}$, (2) MSCs at a density of $2\times106\,\text{cells/mL}$ and (3) a mixed of HUVECs and MSCs (ratio 1:1) at a density of $2\times106\,\text{cells/mL}$. The fibrin bio inks were then loaded into low-temperature printer heads and allowed to equilibrate for 30 min at a $22\,^{\circ}\text{C}$. Printed constructs were crosslinked in $100\,^{\circ}\text{U}$ thrombin for $30\,\text{min}$, rinsed in Phosphate Buffer Saline (PBS), and incubated in serum-free basal media for $48\,\text{h}$.

2.3. MACS-mediated selection of HUVECS

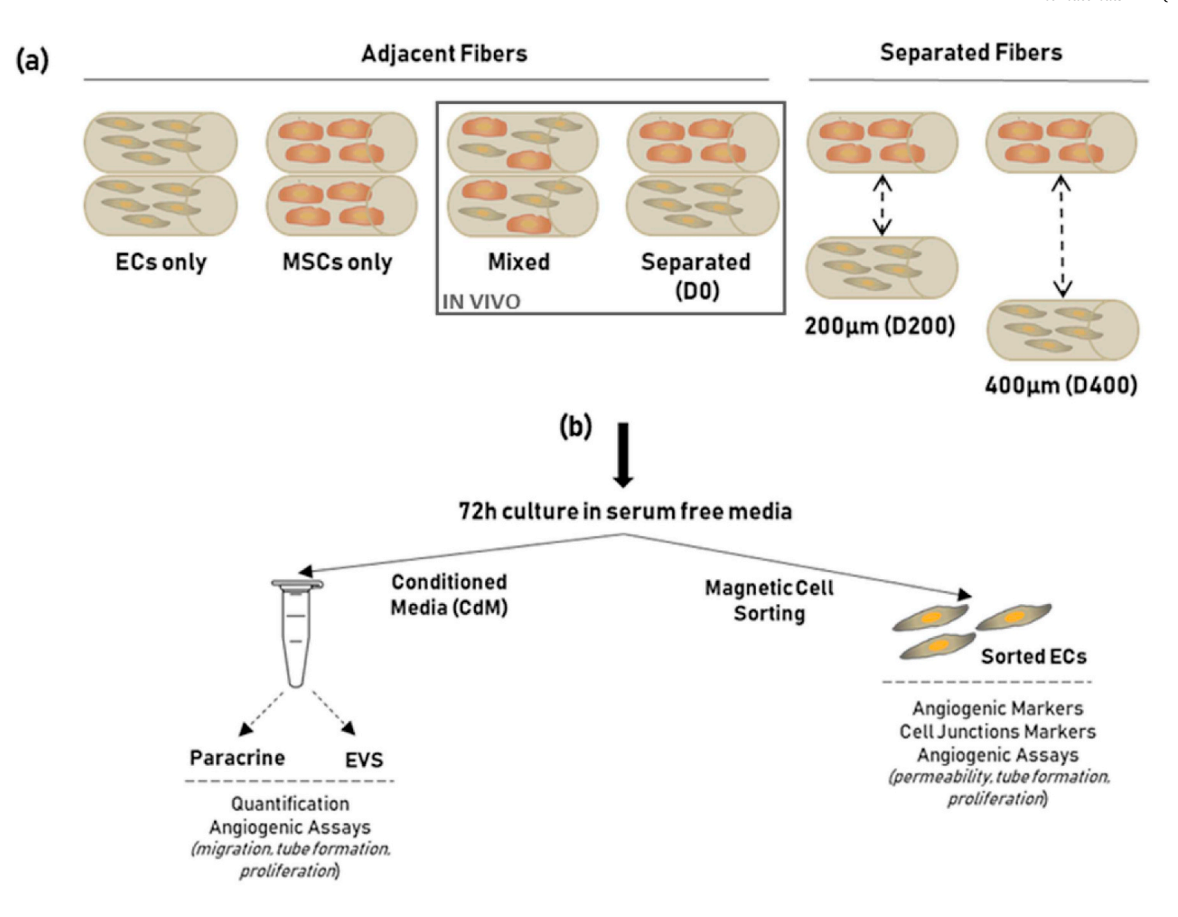
Cell samples from each group were isolated from fibrin hydrogels after 48 h coculture by dissolution in 1 mg/ml collagenase (Sigma) for 30 min at 37 °C and a cell pellet was formed by centrifugation and washed with PBS three times. HUVECs were positively selected for CD31 by magnetic cell sorting (MACS) using MS separation columns (Miltenyi Biotech, Bergisch Gladbach, Germany). Following instructions provided by the manufacturer, a positive selection for ECs using the CD31 MicroBead Kit (Miltenyi) was performed. PBS was used for the final washing step and elution from the column. The CD31 + population (HUVECs) was used in subsequent assays of endothelial function.

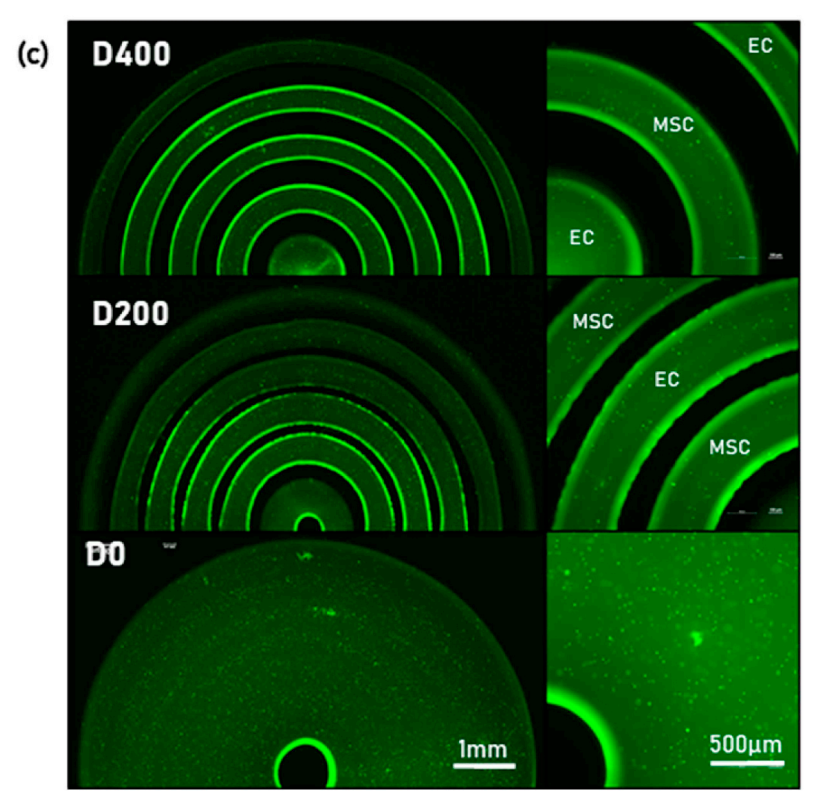
2.4. Flow cytometry (FACS)

Cells sorting was confirmed by flow cytometry prior to use. Harvested and sorted cells were suspended to a concentration of 1×106 cells/mL in cold PBS, 10% FCS, and 1% sodium azide. $10\,\mu\text{g}/$ mL of FITC conjugated anti-CD31 antibody (Abcam, Cambridge, UK) was added to the suspension and incubated for $30\,\text{min}$ in the dark, at room temperature. Cells were then washed 3 times by centrifugation at 400~x g for $5\,\text{min}$ before being resuspended. Flow cytometry was performed on a BD FACSCelesta.

2.5. Quantitative reverse transcriptase polymerase chain reaction (rt-PCR)

Total RNA from HUVECs obtained after MACS-mediated separation was isolated using the RNeasy Plus Mini Kit (Qiagen), following the supplier's protocol (n=9). Reverse transcription was performed using TaqMan Reverse Transcription reagents (Applied Biosystems) following the supplier's protocol. qRT-PCR was performed using TaqMan PCR Master mix and TaqMan Gene Expression Assays for vascular endothelial growth factor-A (VEGF), platelet and endothelial cell adhesion molecule-1 (PECAM), von Willebrand factor (VWF), vascular endothelium cadherin 5 (CDH5), and integrin subunit alpha 5 (ITGA5). Quantification of target gene expression was calculated relative to the reference glyceraldehyde 3-phosphate dehydrogenase (GAPDH) gene. The mean minimal cycle threshold values (Ct) were calculated from triplet reactions.





(caption on next page)

Fig. 1. Methods. (a) Chart showing the different experimental groups: Endothelial Cells (ECs), Mesenchymal Stem Cells (MSCs), Mixed, and Separated with a distance of 0 μm (D0), 200 μm (D200), 400 μm (D400) between fibers. ECs/MSCs groups were used as controls, and are made of adjacent fibers containing only ECs/MSCs, respectively. To investigate the effect of separation of cell population, a mixed group was used. The bioink for the mixed group contains both ECs/MSCs, and the fibers are also printed adjacent to each other. To investigate the effect of distance between cell population, 3 groups were used. For the D0, D200, D400 groups, ECs and MSCs are encapsulated in different bioinks, and the fibers are printed alternatively and with a distance of 0, 200, 400 μm between them. The Mix and Do groups were eventually chosen for in vivo experiments. (b) After printing, 3D printed samples were incubated for 48 h in serum free media. After 48 h, the media was collected and the ECs from the samples were magnetically sorted. (c) Micrographs of 3D printed samples (D0, D200, D400). All samples are 8 mm diameter and 1 mm thick discs. All samples were stained directly after printing, using calcein, showing live cells in green. Using ImageJ, the distance between fibers was calculated: d (D200) = 195.1 \pm 25.4 μm and d(D400) = 381.7 \pm 25.9 μm.

2.6. Enzyme-linked immunosorbent assay (ELISA)

For all experimental groups reported in Fig. 1a, conditioned media (CdM) was collected after 72 h of incubation. CdM media was concentrated using 100 kDa MWCO cut-off filters (Spin-X UF Concentrator, Corning, NY). ELISA kits (Abcam, Cambridge, UK) were used, as per manufacturer instructions, to quantify VEGF, fibroblast growth factor (FGF), angiopoietin 1 (Ang-1) and insulin-like growth factor 1 (IGF1) concentration in the concentrated CdM.

2.7. EVs collection and quantification

EV-containing conditioned media (CdM) was collected after the samples were incubated for 72 h. EVs were then isolated from the CdM via differential centrifugation as reported previously [19]. After initial centrifugation steps to remove cellular debris and larger vesicles, EVs were pelleted in a final 118,000 x g ultracentrifugation step. EVs were then resuspended in PBS and washed with Nanosep 300 kDa MWCO spin filters (Pall, NY). EV yield was measured by determining the total protein concentration and particle concentration, via bicinchoninic acid assay (BSA) using the manufacturer's protocol and nanoparticle tracking analysis, respectively. Nanoparticle tracking analysis was performed using a Nanosight LM10, software version 2.3.

2.8. Functional angiogenic assays

The following assays were performed with at least one of the following conditions: (1) using sorted CD31 $^{+}$ HUVECs and EBM-2 Basal Medium (Lonza) supplemented by EGM-2 SingleQuot Kit, (2) P4 HUVECs (Lonza) and serum-free basal media supplemented with 10% CdM, or (3) P4 HUVECs (Lonza) and serum-free basal media supplemented with 50 $\mu g/ml$ EVs. P4 HUVECs with full EBM-2 media were used as a positive control, and P4 HUVECs with unsupplemented basal media were used as a negative control.

Proliferation Assay. HUVECs were seeded in 24 well plates at a density of 15,000 cells per well and incubated for 36 h. Images of the wells were taken using an inverted microscope (Nikon Eclipse Ti2) and analyzed using ImageJ to measure the confluency (i.e cell surface area).

Migration Assay. The scratch wound assay is a method used to quantify ECs migration. It is based on the ability of EC to fill an area that has been 'wounded' using a pipette tip on a confluent monolayer of ECs [18]. HUVECs were seeded in 48 well plates at a density of 30,000 cells per well, and incubated for 24 h or until a uniform monolayer was formed. The monolayer was then "scratched" using a pipette tip to create a linear gap through the middle of each well. Medium (EBM-2, CdM or EVs) was added. Images of the wells were taken using an inverted microscope (Nikon Eclipse Ti2) after 0 h and 12 h of incubation. Pictures were analyzed using ImageJ to determine the overall gap closure, as previously described [20].

Tube Formation Assay. In vitro assays that simulate the formation of capillary-like structures can be used to investigate late stages of the angiogenic process [21]. 96 well plate was coated with 35 μ l of Matrigel (Corning, NY) and allowed to crosslink for 30 min at 37 °C. HUVECs were seeded in coated 96 well plates at a density of 15,000 cells per well and incubated for 18 h. Images of the wells were taken using an inverted microscope (Nikon Eclipse Ti2) and analyzed using ImageJ

and Angiogenesis Analyzer plugin [22] to measure the confluency (i.e cell surface area).

Permeability Assay. 24 well plates and 0.4-mm pore size inserts were obtained from BD Biosciences. HUVECs were seeded at 60,000 cells per insert well in a total volume of 1.5 mL of EBM-2 media and incubated overnight to allow the cell to form a uniform monolayer. HUVECs monolayer permeability was tested by adding 150 μL of 10 mg/mL 40-kDa fluorescein isothiocyanate (FITC)-Dextran (Sigma-Aldrich) to the upper chamber of each well. Media samples were taken in the bottom chamber of the well after 5, 60, 120, 240min. Measurements were determined with a Spark Multimode Microplate Reader (Tecan) using excitation and emission wavelengths of 485 and 530 nm, respectively.

2.9. Animal implantation

The Institutional Animal Care and Use Committee of the University of Maryland approved the study (protocol number R-MAY-18-26), and all animals were treated in accordance with the Guide for the Care and Use of Laboratory Animals. The experiment was conducted in 30 male adult Sprague Dawley rats.

Implantation was explained elsewhere [23]. Briefly, the fur on the bridge of the snout between the eyes to the caudal end of the calvarium was shaved to expose the surgical site. Using a scalpel, an incision of approximately 1.5 cm was made over the scalp to visualize the calvarium. The underlying bone was exposed. The calvarium was scored with a surgical drill while being irrigated with sterile normal saline to form an 8 mm diameter defect on the sagittal suture. Once the calvarium was freed, it was raised of the dura to finish the defect. The defect was washed with sterile normal saline to remove any debris and/ or bone chips. The scaffold was placed into the defects and the wound was closed over the implant using a running 4-0 monocryl suture. Control animals (CT) underwent sham surgery exactly as described but without implanting the scaffold material. For these animals undergoing cranial window implantation, after a scaffold was placed inside the defect, a circular glass coverslip was placed to cover the implant. The optical window was sealed to the skull with cyanoacrylate, covering all the exposed skull, wound margins and cover glass edges [24]. Animals were monitored daily for up to 12 weeks. No complications were reported.

2.10. Histological analysis

At 4 and 12 days post implantation, animals were euthanized by inhalation of CO2 and the samples and surrounding bone tissue were explanted. Each explanted tissue sample was fixed in paraformaldehyde (4%) for 24 h. Explanted tissue samples were then decalcified embedded in paraffin and prepared for histological analysis by Histoserv, Inc. (Germantown, MD). For histological evaluation, 15 μm thick sections were rehydrated in consecutive ethanol washes and stained by Masson's trichrome staining and Hematoxylin/Eosin. The thickness of the defect, the length of the newly formed bone and the number of blood vessels per area for each sample were measured using ImageJ.

2.11. Optical coherence tomography data acquisition and processing

All animals were placed under anesthesia before OCT imaging. A frequency-domain OCT imaging system was used to follow bone regeneration through out the study. The wavelength-swept laser was centered at 1310 nm with a 100 nm bandwidth, as described elsewhere [25]. The output power of the laser source was set to 17 mW and about 50% of the power was emitted from the sample arm to the animal. The signals were reflected from both the sample and reference arms form interference fringes at the fiber coupler, which were then detected by a balanced photodiode detector. Depth-resolved tomography was achieved by performing Fourier transform of the interference fringes. The axial resolution of this system was $\sim\!10\,\mu\mathrm{m}$ and the lateral resolution was $\sim\!20\,\mu\mathrm{m}$. An 8 mm \times 5 mm field of view (FOV) was imaged by an XY scanner with a speed of $\sim\!10\,\mathrm{s}$ per 3D volume with 704×512 x 496 (X-Z-Y) pixels.

2.12. Statistical analysis

Both biological and technical triplicates were used for all in vitro tests. For histology quantification, the length of new bone formed was calculated over 3 different sections/samples: a total of 9 measurements (n = 12) were taken for each group. For both the thickness of the defect and the number of blood vessel per area, measurements were taken in two different areas/section, with 3 sections/sample: a total of 18 measurements were taken for each group. Data were analyzed using single factor analysis of variance (ANOVA) followed by Tukey's Multiple Comparison Test assuming normal data distribution with a confidence of 95% (p < 0.05).

3. Results and discussion

3.1. HUVECs grown \leq 200 μ m from ECs condition show characteristics of later stage angiogenesis.

The first objective of this work was to study the angiogenic potential of ECs grown in different co-culture conditions, i.e. separated from MSCs by various distances (0, 200 μ m, 400 μ m). After 48 h of incubation, cells were isolated from the 3D printed samples (Fig. 2a). HUVECs uniformly express high levels of CD31. As determined by fluorescence-activated cell sorting analysis, MACS separation of MSC-HUVEC co-cultures yields a very pure population of CD31 HUVECs (Fig. 2b), with an average purity of 94.6 \pm 1.8%, which was subsequently tested using qPCR and angiogenic assays.

Fig. 2c shows the expression of three angiogenic markers (VEGFA, FGF2, and ANG1) in all experimental groups. ECs grown by themselves were used as a control. All three groups with separated cell populations (D0, D200, and D400) showed an increase in gene expression of VEGFA and FGF-2 when compared to the mixed group; with D400 samples showing the most up-regulation of both genes. However, only D0 and D200 samples showed an important increase in fold change for Ang-1. Sorted HUVECs were also used to study proliferation (Fig. 2d). Both mixed and D400 samples showed a significant increase in confluency (p < 0.05) when compared to the positive control. D400 sample's cells showed the most mitotic activity, with a significantly higher proliferation rate.

rt-PCR was also performed to study the expression of genes associated with cellular junctions: ITGA5 (integrin) and CDH5 (VE-cadherin). VE-cadherin was the most up-regulated in D0 and D200 groups while ITGA3 was up-regulated with a higher expression in D400 groups (Fig. 2e). Finally, permeability assays were performed. Fig. 2e shows that monolayers, from cells isolated from D400 samples, were significantly the most permeable than monolayers from D0 and D200 cells.

Angiogenesis is a complex, multistep process that includes endothelial cell proliferation, guided migration, the formation of tubular structures, and stabilization of newly formed vessels by deposition of the basement membrane [26,27]. This process is highly regulated and involves numerous factors [28]. In response to angiogenic stimuli, such as VEGF or FGF-2, ECs turn from a quiescent to an active phenotype characterized by a high mitotic index and increased capacity for migration and matrix proteolysis [29]. Proteolytic enzymes produced and secreted by endothelial cells, such as Matrix metalloproteinase (MMP) family members, lead to cell-directed matrix degradation and remodeling, and they further growth factor delivery of matrix-bound growth factors. The early stages of angiogenesis, proliferation, and migration, in addition to VEGF and FGF-2, are also regulated by angiopoietin-2 (Ang-2). Ang-2 released from activated ECs can bind to its receptor Tie-2, promoting vascular destabilization and a change in ECs adhesive properties [30].

VE-cadherin is an adhesion molecule that mediates cell-to-cell contact between endothelial cells and not only plays a relevant role in the maintenance of vascular integrity but also limits endothelial cell proliferation [31]. When ECs migrate during vessel sprouting, VE-cadherin junctions are temporarily dissolved. Once tubular structures are formed ECs suppress their motile phenotype and new adhesive interactions are established [32]. Integrins, in particular, the $\alpha 5$ subunits, are cell-surface receptors of specific ECM molecules that assist ECs to build new vessels and are strongly linked to the initial steps of angiogenesis. Integrins expressed by ECs is stimulated by angiogenic growth factors, such as FGF-2 [33], and facilitate EC adhesion to the extracellular matrix and their migration [34]. Ang-1, a later marker of angiogenesis, exerts a vessel-sealing effect, by stabilizing the endothelium and reducing integrins expression [35].

The results presented in Fig. 2 suggest that HUVECs grown farther apart from MSCs (D400) are at an earlier stage of angiogenesis (migration/proliferation) than D0/D200 cells. Indeed, results showed an increase in the up-regulation of VEGF, FGF-2, and ITGA3 (integrins) but a smaller fold change in the expression of VE-Cadherin and Ang-1. HUVECs isolated from D400 samples were also still highly proliferative when compare to D0/D200 cells. On the contrary, HUVECs incubated closer ($\leq 200\,\mu m$) to MSCs, started to show signs of stabilization, mainly an increase in Ang-1 and VE-cadherin expression.

The crosstalk between hMSC and HUVECs is regulated by the separation and distance of cell populations.

The second objective of this work was to investigate whether several soluble factors that may influence HUVECs behavior are differentially secreted by cells grown in different 3D printed coculture for 48 h (Fig. 3a). The concentration of three common growth factors (VEGFA, FGF2, and Ang-1) was measured using ELISA (Fig. 3b and Supplemental Fig. I). Results indicates a significant increase (p < 0.05) in VEGFA and FGF2 secretions between MSCs cultured in isolation (731 ± 84 pg/ ml and 495 \pm 43 pg/ml respectively) and ECs cultured in isolation $(306 \pm 10 \text{ pg/ml} \text{ and } 227 \pm 69 \text{ pg/ml} \text{ respectively})$. In addition, VEGFA and FGF2 were secreted at a significant higher rate by HUVECs and MSCs in "mixed" coculture than HUVECs alone; both concentrations were even higher than the average of ECs alone and MSCs alone, confirming that co-culture improves paracrine secretion of ECs. Those findings are widely supported by literature: MSCs have been shown to be pro-angiogenic, and be able to activate ECs that will in return secrete more VEGFA and FGF2 [36-38]. The levels of VEGFA and FGF2 in D0/ D200 CdM was also significantly higher than the ones from "mixed" cocultures. In addition, Ang-1 levels are significantly higher in D0/ D200 groups (p < 0.05). Those results match the qPCR results found in Fig. 2c: D0/D200 coculture cells show both an up-regulation of Ang-1 gene and an increased secretion in Ang-1 when compared to cells from D400 groups. However, D400 CdM contained significantly lower levels of both VEGFA and FGF2 (p < 0.05), while it was previously shown that the gene for both of those growth factors was the most up-regulated. This suggests that genetic material is not being transduced into proteins or that VEGFA and FGFs are not being secreted via paracrine signaling by the cells in the D400 group, but most likely using another mode of cell-cell communication, such as the exchange of exosomes.

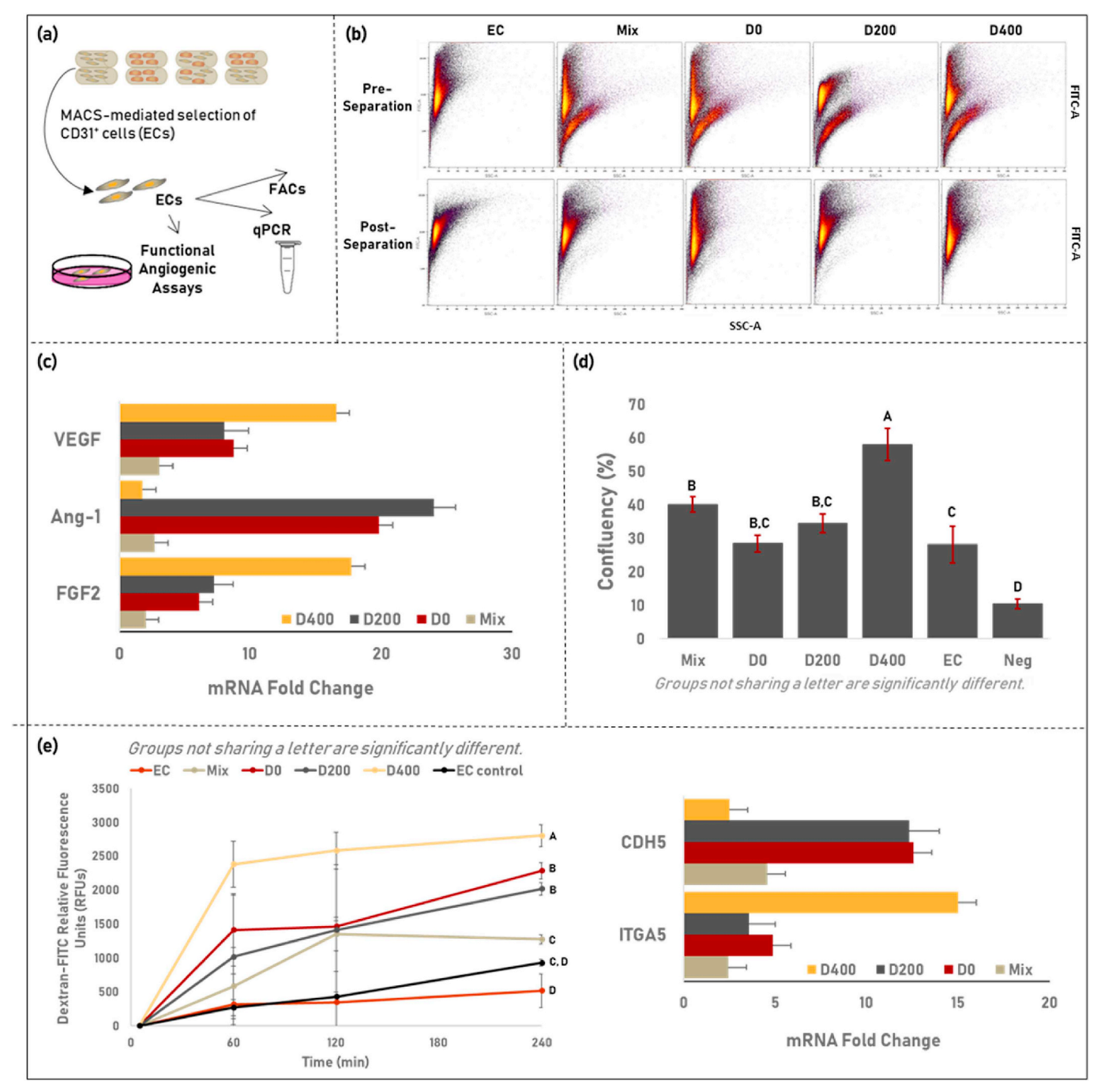


Fig. 2. ECs grown in close ($\leq 200 \, \mu m$) coculture condition show characteristics of a later stage angiogenesis. For all figures, groups not sharing a letter are statistically different. (a) Schematic of the experiment. Cells were collected from the 3D printed samples after 48 h of incubation. HUVECs were sorted using CD31 MACS, and used in subsequent experiments. (b) FACS analysis, pre and post-separation. The bottom row confirms the positive selection of HUVECs (c) Rt-PCR (n = 9) showed an increase in gene expression of VEGF and FGF-2 for cells isolated from D400 samples and an increase in the fold change in mRNA of Ang-1 for cells isolated from D0/D200 samples. (d) Cell confluency (n = 3) after 24 h of incubation. D400 cells exhibit a significantly higher proliferation rate (p < 0.05) than the other groups. (e) Permeabilization Assay (n = 3). Diffusion of Dextran-FITC was observed through a confluent monolayer of HUVECs. Cells isolated from D400 samples showed the highest permeability. Rt PCR showed an increase in gene expression of ITGA5 for the same cells.

A second set of experiments was conducted to investigate whether CdM modulated cell viability (Fig. 3c) and migration (Fig. 3d) of HUVECs from different co-culture conditions. The proliferation of HUVECs was significantly stimulated when cultured with CdM media regardless of the type of coculture, as compared to the negative control or CdM from ECs and MSCs cultured in isolation. However, no significant difference was observed between groups supplemented with CdM from "mixed", D0, D200 and D400 cocultures. HUVEC migratory activity when cultured with CdM increased with distance between co-cultured

HUVECs and hMSC. Quantification of the invaded area indicated that wound closure was significantly higher in D400 co-cultures (p < 0.05) than D0 or "mixed" cocultures.

Tube formation assays showed that HUVECs grown with medium supplemented with CdM from all coculture groups self-assembled and elongated, forming a capillary-like network with typically closed structures similar to the ones observed in the positive control group (Fig. 3e). Incubation of HUVECs with CdM from D0 and D200 groups resulted in a longer network of tube-like structures.

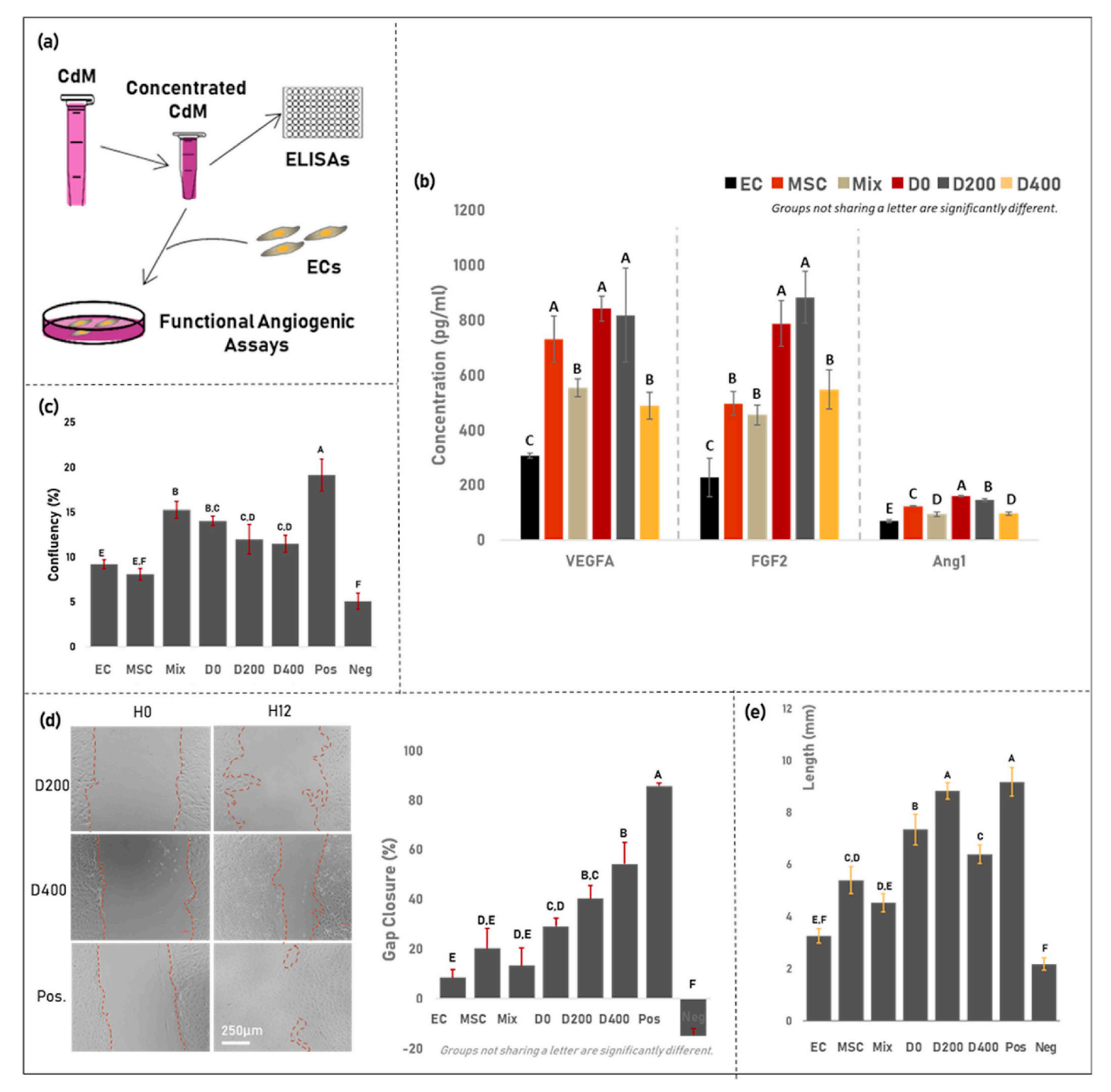


Fig. 3. The crosstalk between hMSC and HUVECs is regulated by the separation and distance of cell populations. Groups not sharing a letter are significantly different. (a) Schematic of the experiments. After 48 h of incubation, CdM was collected and concentrated. Different growth factors concentration was measured using ELISAs. Finally the CdM was used to supplement media in functional Angiogenic assays. (b) Concentration of VEGFA, FGF-2 and Ang-1 in CdM from all experimental groups (n = 9). For each growth factor, groups not sharing a letter are statistically different (p < 0.05). Paracrine secretions were significantly increased in coculture groups where HUVECs were separated from MSCs (D0, D200). (c) CdM was used to supplement media in a proliferation assay (n = 3). HUVECs confluency after 24 h was measured. No statistical difference was observed between coculture groups. (d) CdM was used to supplement media for migration assay (n = 3). Picture of the wound were taken 12 h after "scratching" a confluent monolayer of HUVECs, and the wound closure was calculated. Groups incubated with CdM from coculture in which HUVECs and MSCs were grown the farther apart (D400) show a significant increase (p < 0.05) in migratory activity. (e) CdM was used to supplement media for a tube formation assay (n = 3). HUVECs incubated with CdM from coculture in which HUVECs and MSCs were grown separated but close (< 200 μ m) (D0, D200) formed a significantly longer network (p < 0.05).

Those findings seem to support the data collected in Fig. 2 and 3b. D0/D200 CdM preferentially promotes tube formation, a later stage of angiogenesis, due in part to a significant increase in Ang-1 paracrine secretion. While CdM from D400 samples contains a lower concentration of VEGF/FGF than D0 or D200, it still significantly increased HUVECs migration in a wound assay. This seems to further confirm that

HUVECs grew in close ($\!\leq\!200\,\mu m)$ coculture condition show characteristics of a later stage angiogenesis.

Oxygen gradients throughout the samples could potentially have an impact on cell communication, but when the distance between 3D printed fibers is less than 500 µm, it has been shown that the difference in oxygen is not significant [39]. However, since MSCs cultured in

isolation produced more VEGFA and FGF2 than HUVECs cultured in isolation, separating cell populations in different fibers (D0, D200, D400) could create a gradient of paracrine secretions. And this gradient could also vary depending on the distance between fibers. This phenomenon could explain the difference in VEGF/FGF secretion between "mixed", D0, D200, and D400 groups. Endothelial cell migration is mediated by VEGF gradients which orientates, attracts, and induces proliferation of new blood vessels [40-42]. Furthermore, the shape of the VEGFA gradient can dictate the proliferation and migratory response exhibited by endothelial cells [43]. Models predict that VEGF distribution along the gradient forms an uneven slope: cells close to the VEGF-A source would be in an exponential high concentration zone. while cells further away from the source would be in a zone of linear low concentration [44]. In addition, analysis of cell migration in different regions of the applied gradients showed that cells efficiently interpret the positional information provided by the gradients [43]: responses for both VEGFA and FGF2 were more pronounced in the exponential regions of the gradients compared with the linear regions. Based on those findings, we could hypothesize that D0/D200 cocultures formed stronger gradients, eliciting a stronger response from HUVECs to MSCs paracrine secretion.

3.2. EV cargo increases with distance between cell populations and promotes early angiogenesis

The third objective of this work was to study the angiogenic potential of extracellular vesicles (EVs) exchanged between cell populations. Many studies indicate EVs is a key mediator of the therapeutic functions imparted by cell therapies [45-47]. Thus, we investigated whether EVs play a role in the angiogenic effects observed with CdM. The specific subset of EVs analyzed in this study was influenced by the isolation method, which separated vesicles by size. Here, we are looking at smaller EVs averaging around 150 nm and larger vesicles are removed during the isolation process. Consequently, the CdM will contain a combination of the extracellular vesicles observed in Fig. 4 and other larger vesicles. While it is possible that these larger EV populations have similar effects as the ones we later isolated, studies have also suggested that subpopulations of EVs have different compositions and functions [48,49]. . It has been shown that when isolated EVs by density gradient, the low and high density EVs have distinct protein and RNA profiles leading to different effects on target cells. In addition to size and density, subpopulations based on surface composition also show differential functions. To have a clear understanding of the role of different EVs, separate future studies analyzing various subpopulations are necessary.

Here EVs were isolated from the CdM using differential centrifugation and quantified (Fig. 4a). The results showed a significant increase (p < 0.05) in protein concentration per EVs in all separated co-culture groups (D0, D200, D400) as compared to EVs only. EVs collected from D400 CdM showed the most increase in protein concentration when compared to D0 or D200 groups. Which seems to suggest that EVs cargo content increases with the distance between HUVECs and MSCs. Fig. 2c indicated that ECs grown in D400 coculture conditions showed an important up-regulation of VEGFA and FGF2 genes. However, no significant increase in VEGF or FGF secretions were observed in the CdM. Altogether, it would indicate that most likely VEGF/FGF proteins or nucleic acids regulating these pathways were preferentially loaded into EVs in D400 cocultures. We could hypothesize that EVs secretion is preferred as a mode of cell-cell communication when cell populations are further apart.

Tube formation (Fig. 4c), proliferation (Fig. 4d) and migration (Fig. 4e) assays were performed to assess the angiogenic potential of EVs only. Results indicated that media supplemented with D400 EVs significantly improved HUVECs proliferation and migration in comparison to Mix, D0, or D200. HUVECs proliferation after 24 h seemed to be correlated to EV proteins concentration (r [2] = 0.9551) (Fig. 4d).

However, no significant effect on tube formation was observed. As discussed previously, VEGF and FGF are both involved in early angiogenesis, promoting EC proliferation and migration. Those results would further suggest that either VEGF/FGF or other nucleic acids involved in these pathways were loaded in EVs for farther apart co-culture (D400).

Evidence seems to indicate that in coculture where cells are the farther apart, EVS is preferred for cell-cell communication. This could explain why angiogenesis is happening slower than groups D0, D200. This study appears to indicate that EVs are largely involved in cell-cell communication in cocultures where the cells are farther apart, while paracrine signaling via soluble proteins is dominant when the cells are closer together. The mode of cell-cell communication may dominate the rate of angiogenesis. VEGF, FGF-2, and Ang1 can act upon target cells by interacting with receptors on the cell surface. Depending on whether the function of these EVs is imparted by surface proteins or internal cargo, they may need to initially be processed before triggering a functional response, consequently resulting in delayed angiogenesis. Thus, cocultures with cell populations closer together demonstrated later stage angiogenesis.

3.3. Healing of critical-size bone defect was improved using optimized 3DP scaffolds (D0 scaffolds)

In the in vitro experiments, we observed that HUVECs and MSCs cultured in separate fibers, but at a distance less than 200 μm (D0, D200 groups) presented signs of later angiogenesis, suggesting that maybe the angiogenesis process was happening faster than when the cell populations were separated by 400 μm (D400 group) or mixed together (Mix group). The D0 group was then used in the in vivo study to investigate if angiogenesis and neovascularization could be improved in a cranial model, as compared to Mix group, and therefore improve bone formation.

In order to evaluate the potential of our optimized 3D printed cocultures scaffolds for neovascularization and consequent bone regeneration in vivo, 8-mm bone defects were created in the calvarial bone of rats. Two experimental groups (Mix and D0) and one control group (CT, sham surgery, no implant) were assessed twelve weeks postsurgery. Live/Dead staining was performed in order to verify the viability of the cells post-printing, and prior to implantation. Fluorescent images showed mostly viable cells (Supplemental Figure IIIa). In order to confirm the proper patterning of the cells, rMSCs and rECs were stained with Calcein AM or DAPI respectively, prior to printing. After printing, samples were imaged (Supplemental Figure IIIb) and confirmed that two distinct cell populations were in separate fibers. After implantation, all wounds healed without any complications, or evidence of infection. At retrieval, samples appeared to be covered by a healthy periosteum. No signs of inflammation were visible. On visual examination (Supplemental Figure IV), the critical size defect left unfilled (CT) was not closed, the sagittal vein and peripheral blood vessels were clearly visible. New tissue formation was visible only on the edges of the defect. Defects in both Mix and D0 group appeared to have nearly closed. However, the sagittal vein was still slightly visible in the Mix group, suggesting that the newly formed tissue might be thinner than in the D0 group.

The densities of blood vessels present in all scaffolds were measured 4 weeks after implantation. Histological sections stained with HE showed relatively few blood vessels within the control scaffolds (Fig. 5a). In contrast, 3DP scaffolds displayed a higher density of blood vessels interspersed throughout the scaffold. Quantification of blood vessels densities confirmed that D0 scaffolds had a significantly higher blood vessel density (p < 0.05) than Mix scaffolds and CT scaffolds (Fig. 5b).

The effect of induced angiogenesis on bone tissue regeneration within the critical-sized defects after 12 weeks were analyzed next. Histological analysis of the samples was performed using a Masson's trichrome stain (Fig. 5c). Gross observations of the Masson's trichrome

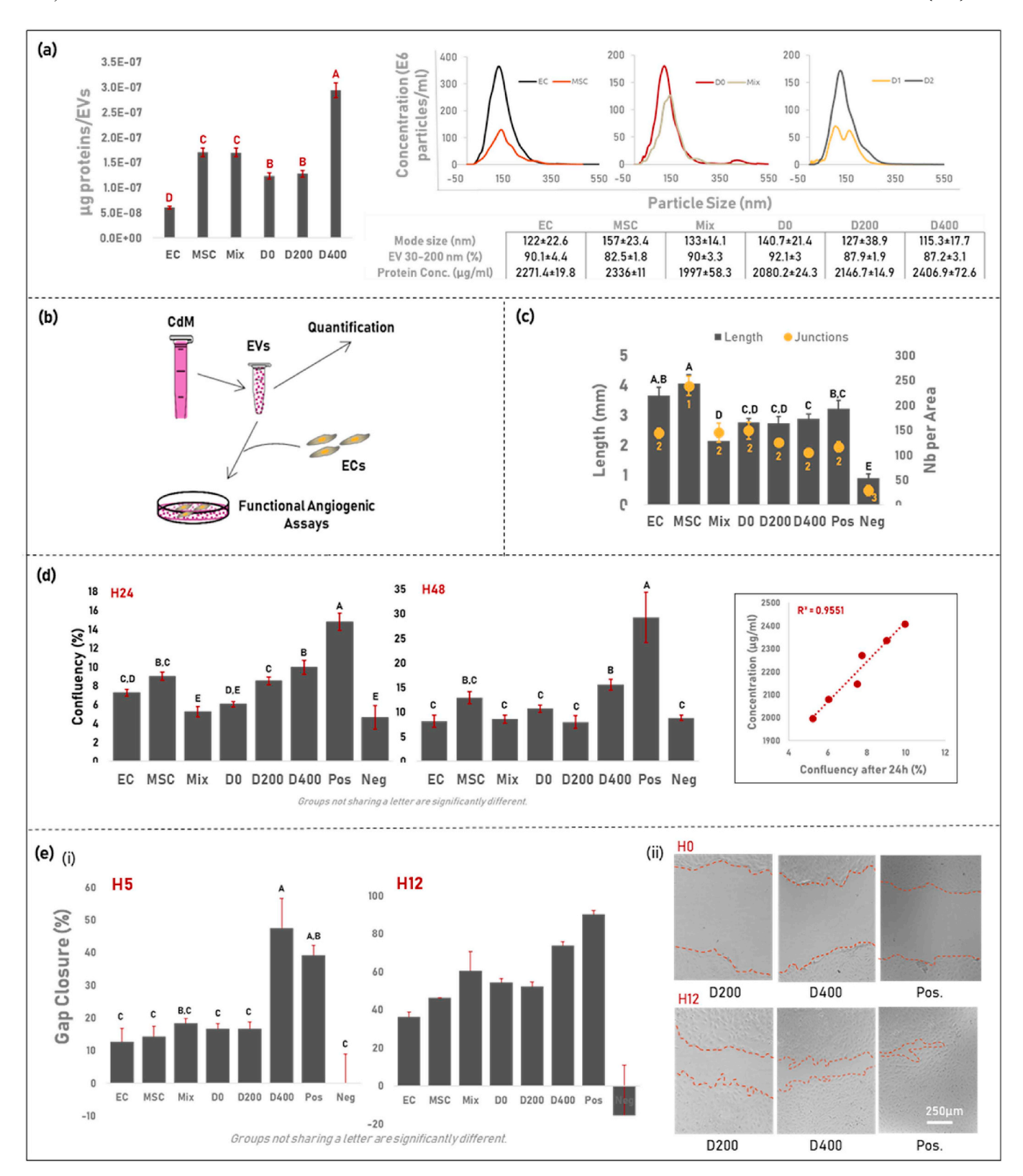


Fig. 4. EVs cargo increases with distance between cell populations and promotes early angiogenesis. For each figure, groups not sharing a letter are significantly different (p < 0.05). (a) EVs and protein per EVs quantification (n = 3). Proteins concentration per EVs increases with the distance between cell populations in co-culture. (b) Schematics of experiment. After 48 h of incubation, CdM was collected from all experimental groups and EVs were collected by centrifugation. EVs were then quantified and their Angiogenic potential was evaluated in functional Angiogenic assays. (c) Tube Formation Assay (n = 3). EVs supplemented media was used to incubate HUVECs on Matrigel. Total length of network formed by tube like structures was measured. No statistical difference was observed between coculture groups. (d) Proliferation Assay (n = 3). EVs supplemented media was used to grown HUVECs. Confluency was measured after 24 and 48 h of incubation. HUVECs grown with D400 EVs showed a higher proliferation rate. (e) Migration Assay (n = 3). HUVECs grown in D400 EVs supplemented media showed a faster migration.

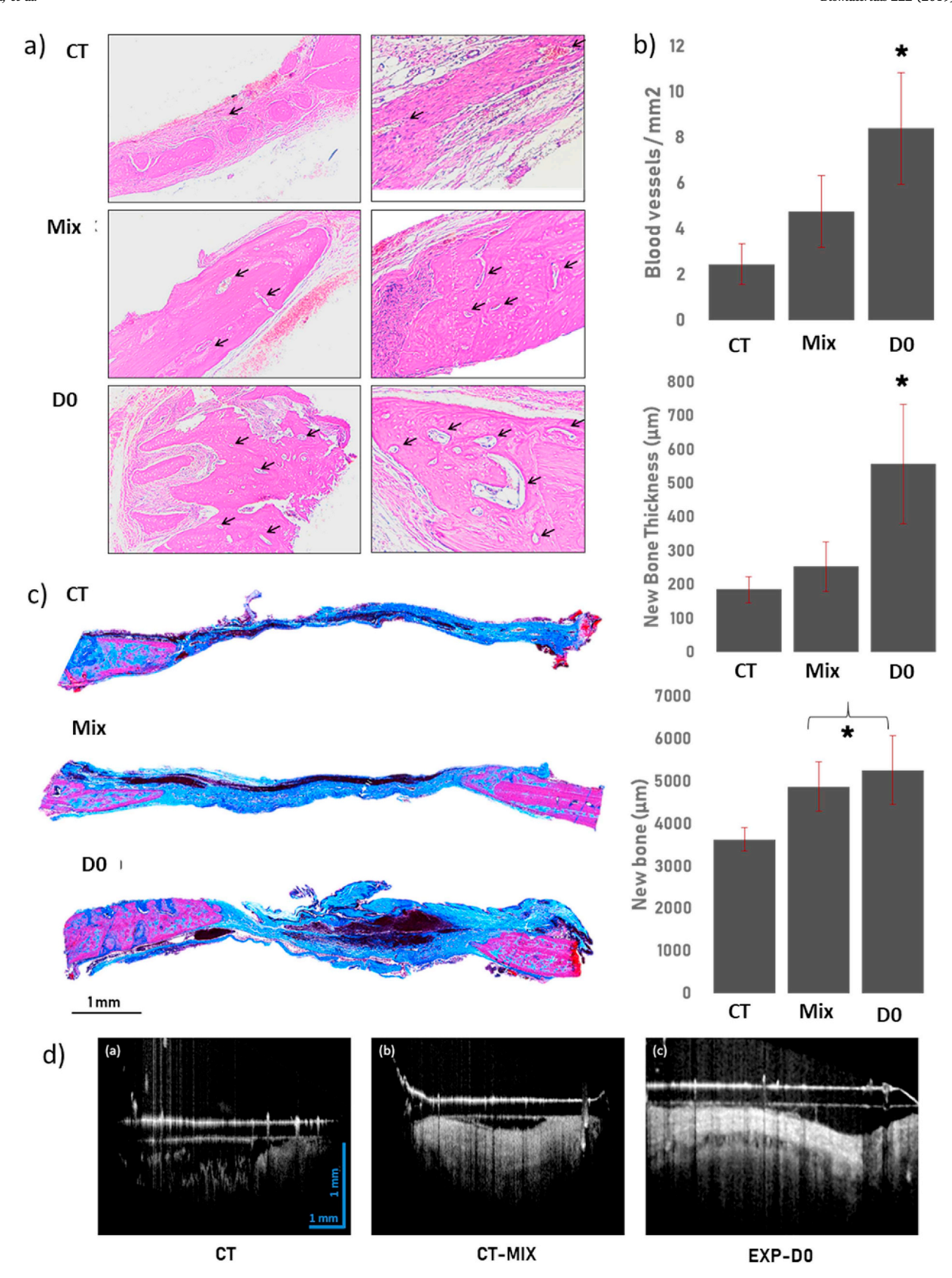


Fig. 5. Healing of critical-size bone defect was improved using optimized 3DP scaffolds (D0 scaffolds) (a) Representative images of H&E staining after 4 weeks. The black arrows are pointing to blood vessels. (b) Histomorphological quantification of blood vessels/mm [2], new bone formation and new bone thickness. (c) Masson's trichrome staining of full cross section of the defect. (d) OCT B-Scan images of scaffolds after 4 weeks implantation.

stained slides showed only minimal appositional bone regeneration and a thin layer of fibrous tissue and obvious defects remaining in the control group. Do and Mix samples showed significantly enhanced bone growth as compared to controls ones. Histomorphometric analysis corroborated the histological findings. The length and thickness of the newly formed bone in defect sites was calculated. The results indicated that D0 groups were significantly thicker than the Mix and CT groups. However, the length of new bone was not significantly different from the other groups.

Optical coherence tomography (OCT) is an established biomedical imaging technology for imaging of tissue non-destructively with micron-level resolution. OCT usually can provide < 10 µm resolution and 1–2 mm penetration depth as well as millimeter scale field of view (FOV) [50,51]. In addition, with high-speed Fourier-domain detection techniques, OCT now can acquire a 3D image within 1 s with speed of more than 100,000 A-scan/s [52], and does not require exogenous contrast agents such as fluorescent dyes, which makes it advantageous over other conventional microscopic imaging methodologies. OCT B-Scan images (Fig. 5d) presented several differences across all three groups. Rats with D0 scaffolds showed clearer laminar structures within the defect. However, only homogenous high scattering tissues were shown with Mix scaffolds. Ct groups did not have clear visible structures. These morphological differences could be explained by different rate of osteogenesis and bone formation/mineralization with the defect.

4. Conclusion

Vascularization is a crucial process during the growth and development of bone, and in vitro vascularization strategies can greatly be improved using the coculture of HUVECS and MSCs. Communication between cell population plays an important role in angiogenesis, and can be affected by a variety of factors. However, little is known about the effect of cell patterning and the distance between cell populations on their crosstalk. In the present study, we showed that controlling the distance between ECs and MSCs in co-culture, using 3D printing, could influence angiogenesis. First, we showed that HUVECs grown in close $(\leq 200 \,\mu\text{m})$ co-culture condition presented characteristics of later stage angiogenesis. In addition, the separation and distance between ECs and MSCs seemed to modulate cell-cell communication. In groups in which fibers were printed farther apart (400 μm), cells produced EVs with a significantly increase cargo. Furthermore, by modulating distance between printed fibers, results indicated that we can create different paracrine secretion gradients, hence modulate the crosstalk between HUVECS and MSCs. Finally, in vivo experiment results further suggest that distance between ECs and MSCs in 3DP co-culture can influence angiogenesis and subsequent bone regeneration. Scaffolds in which cell populations were separated by a distance < 200 µm not only presented a significantly higher number of blood vessels, but also were able to regenerate a larger amount of bone defect than the control group. This observation suggests the higher efficiency of indirect ECs/MSCs contact in prompting the release of paracrine signals that stimulate the angiogenesis of local tissues.

Acknowledgments

This work was supported by the National Institute of Biomedical Imaging and Bioengineering / National Institutes of Health (NIBIB/NIH) Center for Engineering Complex Tissues P41 EB023833, and by the U.S. National Institutes of Health under Award No. R01 EB014946.

Appendix A. Supplementary data

Supplementary data to this article can be found online at https://doi.org/10.1016/j.biomaterials.2019.119423.

References

- D.A. Towler, The osteogenic-angiogenic interface: novel insights into the biology of bone formation and fracture repair, Curr. Osteoporos. Rep. 6 (2008) 67–71.
- [2] Y.-C. Huang, D. Kaigler, K.G. Rice, P.H. Krebsbach, D.J. Mooney, Combined angiogenic and osteogenic factor delivery enhances bone marrow stromal cell-driven bone regeneration, J. Bone Miner. Res. 20 (2004) 848–857.
- [3] M. Radisic, J. Malda, E. Epping, W. Geng, R. Langer, G. Vunjak-Novakovic, Oxygen gradients correlate with cell density and cell viability in engineered cardiac tissue, Biotechnol. Bioeng. 93 (2006) 332–343.
- [4] O. Ball, B.-N.B. Nguyen, J.K. Placone, J.P. Fisher, 3D printed vascular networks enhance viability in high-volume perfusion bioreactor, Ann. Biomed. Eng. 44 (2016) 3435–3445.
- [5] B.-N.B. Nguyen, R.A. Moriarty, T. Kamalitdinov, J.M. Etheridge, J.P. Fisher, Collagen hydrogel scaffold promotes mesenchymal stem cell and endothelial cell coculture for bone tissue engineering, J. Biomed. Mater. Res. A 105 (2017) 1123–1131.
- [6] J.T. Egaña, F.A. Fierro, S. Krüger, M. Bornhäuser, R. Huss, S. Lavandero, H.-G. Machens, Use of human mesenchymal cells to improve vascularization in a mouse model for scaffold-based dermal regeneration, Tissue Eng. A 15 (2009) 1191–1200
- [7] B.-N.B. Nguyen, R.A. Moriarty, T. Kamalitdinov, J.M. Etheridge, J.P. Fisher, Collagen hydrogel scaffold promotes mesenchymal stem cell and endothelial cell coculture for bone tissue engineering, J. Biomed. Mater. Res. A 105 (2017) 1123–1131.
- [8] R.L. Dahlin, J.G. Gershovich, F.K. Kasper, A.G. Mikos, Flow perfusion Co-culture of human mesenchymal stem cells and endothelial cells on biodegradable polymer scaffolds, Ann. Biomed. Eng. 42 (2014) 1381–1390.
- [9] J. Ma, J.J.J.P. van den Beucken, F. Yang, S.K. Both, F.-Z. Cui, J. Pan, J.A. Jansen, Coculture of osteoblasts and endothelial cells: optimization of culture medium and cell ratio, Tissue Eng. C Methods 17 (2011) 349–357.
- [10] Y. Yu, J. Mu, Z. Fan, G. Lei, M. Yan, S. Wang, C. Tang, Z. Wang, J. Yu, G. Zhang, Insulin-like growth factor 1 enhances the proliferation and osteogenic differentiation of human periodontal ligament stem cells via ERK and JNK MAPK pathways, Histochem. Cell Biol. 137 (2012) 513–525.
- [11] Z. Huang, P.-G. Ren, T. Ma, R.L. Smith, S.B. Goodman, Modulating osteogenesis of mesenchymal stem cells by modifying growth factor availability, Cytokine 51 (2010) 305–310.
- [12] F. Martín-Saavedra, L. Crespo, C. Escudero-Duch, L. Saldaña, E. Gómez-Barrena, N. Vilaboa, Substrate microarchitecture shapes the paracrine crosstalk of stem cells with endothelial cells and osteoblasts, Sci. Rep. 7 (2017) 15182.
- [13] G. Kasper, N. Dankert, J. Tuischer, M. Hoeft, T. Gaber, J.D. Glaeser, D. Zander, M. Tschirschmann, M. Thompson, G. Matziolis, G.N. Duda, Mesenchymal stem cells regulate angiogenesis according to their mechanical environment, Stem Cells 25 (2007) 903–910.
- [14] F.P. Seib, M. Prewitz, C. Werner, M. Bornhäuser, Matrix elasticity regulates the secretory profile of human bone marrow-derived multipotent mesenchymal stromal cells (MSCs). Biochem. Biophys. Res. Commun. 389 (2009) 663–667.
- [15] C. Piard, H. Baker, T. Kamalitdinov, J.P. Fisher, Bioprinted osteon-like scaffolds enhance in vivo neovascularization, Biofabrication (2019), https://doi.org/10. 1088/1758-5090/ab078a.
- [16] C.M. Piard, Y. Chen, Fisher, J. P. Cell-laden 3D printed scaffolds for bone tissue engineering, Clin. Rev. Bone Miner. Metabol. 13 (2015).
- [17] V. KARAGEORGIOU, D. KAPLAN, Porosity of 3D biomaterial scaffolds and osteogenesis, Biomaterials 26 (2005) 5474–5491.
- [18] C.-C. Liang, A.Y. Park, J.-L. Guan, Vitro scratch assay: a convenient and inexpensive method for analysis of cell migration in vitro, Nat. Protoc. 2 (2007) 329–333.
- [19] T.N. Lamichhane, R.S. Raiker, S.M. Jay, Exogenous DNA loading into extracellular vesicles via electroporation is size-dependent and enables limited gene delivery, Mol. Pharm. 12 (2015) 3650–3657.
- [20] D.B. Patel, K.M. Gray, Y. Santharam, T.N. Lamichhane, K.M. Stroka, S.M. Jay, Impact of cell culture parameters on production and vascularization bioactivity of mesenchymal stem cell-derived extracellular vesicles, Bioeng. Transl. Med. 2 (2017) 170–179.
- [21] I. Arnaoutova, H.K. Kleinman, In vitro angiogenesis: endothelial cell tube formation on gelled basement membrane extract, Nat. Protoc. 5 (2010) 628–635.
- [22] Carpentier, G. ImageJ Contribution: Angiogenesis Analyzer. ImageJ News.
- [23] P.P. Spicer, J.D. Kretlow, S. Young, J.A. Jansen, F.K. Kasper, A.G. Mikos, Evaluation of bone regeneration using the rat critical size calvarial defect, Nat. Protoc. 7 (2012) 1918–1929.
- [24] A. Holtmaat, T. Bonhoeffer, D.K. Chow, J. Chuckowree, V. De Paola, S.B. Hofer, M. Hübener, T. Keck, G. Knott, W.-C.A. Lee, R. Mostany, T.D. Mrsic-Flogel, E. Nedivi, C. Portera-Cailliau, K. Svoboda, J.T. Trachtenberg, L. Wilbrecht, Longterm, high-resolution imaging in the mouse neocortex through a chronic cranial window, Nat. Protoc. 4 (2009) 1128–1144.
- [25] C.-W. Chen, M.W. Betz, J.P. Fisher, A. Paek, Y. Chen, Macroporous hydrogel scaffolds and their characterization by optical coherence tomography, Tissue Eng. C Methods 17 (2011) 101–112.
- [26] H.M. Eilken, R.H. Adams, Dynamics of endothelial cell behavior in sprouting angiogenesis, Curr. Opin. Cell Biol. 22 (2010) 617–625.
- [27] M. Potente, H. Gerhardt, P. Carmeliet, Basic and therapeutic aspects of angiogenesis, Cell 146 (2011) 873–887.
- [28] M.L. Iruela-Arispe, H.F. Dvorak, Angiogenesis: a dynamic balance of stimulators and inhibitors, Thromb. Haemost. 78 (1997) 672–677.
- [29] W. Risau, Mechanisms of angiogenesis, Nature 386 (1997) 671-674.

- [30] M. Scharpfenecker, U. Fiedler, Y. Reiss, H.G. Augustin, The Tie-2 ligand Angiopoietin-2 destabilizes quiescent endothelium through an internal autocrine loop mechanism, J. Cell Sci. 118 (2005) 771–780.
- [31] D. VE-Cadherin Vestweber, Arterioscler. Thromb. Vasc. Biol. 28 (2008) 223-232.
- [32] P. Carmeliet, Angiogenesis in health and disease, Nat. Med. 9 (2003) 653-660.
- [33] P. Brooks, R. Clark, D. Cheresh, Requirement of vascular integrin alpha v beta 3 for angiogenesis, Science 264 (80) (1994) 569–571.
- [34] C.J. Avraamides, B. Garmy-Susini, J.A. Varner, Integrins in angiogenesis and lymphangiogenesis, Nat. Rev. Cancer 8 (2008) 604–617.
- [35] G. Thurston, J.S. Rudge, E. Ioffe, H. Zhou, L. Ross, S.D. Croll, N. Glazer, J. Holash, D.M. McDonald, G.D. Yancopoulos, Angiopoietin-1 protects the adult vasculature against plasma leakage, Nat. Med. 6 (2000) 460–463.
- [36] H. Mayer, H. Bertram, W. Lindenmaier, T. Korff, H. Weber, H. Weich, Vascular endothelial growth factor (VEGF-A) expression in human mesenchymal stem cells: autocrine and paracrine role on osteoblastic and endothelial differentiation, J. Cell. Biochem. 95 (2005) 827–839.
- [37] H. Li, R. Daculsi, M. Grellier, R. Bareille, C. Bourget, M. Remy, J. Amedee, The role of vascular actors in two dimensional dialogue of human bone marrow stromal cell and endothelial cell for inducing self-assembled network, PLoS One 6 (2011) e16767.
- [38] Q. Ge, H. Zhang, J. Hou, L. Wan, W. Cheng, X. Wang, D. Dong, C. Chen, J. Xia, J. Guo, X. Chen, X. Wu, D. Dong, D. Dong, C. Chen, C. Chen, J. Xia, J. Xia, J. Guo, J. Guo, X. Chen, X. Chen, X. Wu, X. Wu, VEGF secreted by mesenchymal stem cells mediates the differentiation of endothelial progenitor cells into endothelial cells via paracrine mechanisms, Mol. Med. Rep. 17 (2017) 1667–1675.
- [39] S.C. Lesher-Pérez, G.-Á. Kim, C. Kuo, B.M. Leung, S. Mong, T. Kojima, C. Moraes, M.D. Thouless, G.D. Luker, S. Takayama, Dispersible oxygen microsensors map oxygen gradients in three-dimensional cell cultures, Biomater. Sci. 5 (2017) 2106–2113.
- [40] C.-L.E. Helm, M.E. Fleury, A.H. Zisch, F. Boschetti, M.A. Swartz, Synergy between Interstitial Flow and VEGF Directs Capillary Morphogenesis in Vitro through a Gradient Amplification Mechanism, (2005).
- [41] H. Gerhardt, M. Golding, M. Fruttiger, C. Ruhrberg, A. Lundkvist, A. Abramsson, M. Jeltsch, C. Mitchell, K. Alitalo, D. Shima, C. Betsholtz, VEGF guides angiogenic sprouting utilizing endothelial tip cell filopodia, J. Cell Biol. 161 (2003) 1163–1177.

- [42] N.C. Rivron, E.J. Vrij, J. Rouwkema, S. Le Gac, van den Berg, A, R.K. Truckenmüller, C. A. van Blitterswijk, Tissue deformation spatially modulates VEGF signaling and angiogenesis, Proc. Natl. Acad. Sci. 109 (2012) 6886–6891.
- [43] I. Barkefors, S. Le Jan, L. Jakobsson, E. Hejll, G. Carlson, H. Johansson, J. Jarvius, J.W. Park, N. Li Jeon, J. Kreuger, Endothelial cell migration in stable gradients of vascular endothelial growth factor A and fibroblast growth factor 2: effects on chemotaxis and chemokinesis, J. Biol. Chem. 283 (2008) 13905–13912.
- [44] A. Akeson, A. Herman, D. Wiginton, J. Greenberg, Endothelial cell activation in a VEGF-A gradient: relevance to cell fate decisions, Microvasc. Res. 80 (2010) 65–74.
- [45] C. Lee, S.A. Mitsialis, M. Aslam, S.H. Vitali, E. Vergadi, G. Konstantinou, K. Sdrimas, A. Fernandez-Gonzalez, S. Kourembanas, Exosomes mediate the cytoprotective action of mesenchymal stromal cells on hypoxia-induced pulmonary hypertension, Circulation 126 (2012) 2601–2611.
- [46] P. Prathipati, S.S. Nandi, P.K. Mishra, Stem cell-derived exosomes, autophagy, extracellular matrix turnover, and miRNAs in cardiac regeneration during stem cell therapy, Stem Cell Rev. 13 (2017) 79.
- [47] S. Sahoo, E. Klychko, T. Thorne, S. Misener, K.M. Schultz, M. Millay, A. Ito, T. Liu, C. Kamide, H. Agrawal, H. Perlman, G. Qin, R. Kishore, D.W. Losordo, Exosomes from human CD34 ⁺ stem cells mediate their proangiogenic paracrine activity, Circ. Res. 109 (2011) 724–728.
- [48] E. Willms, H.J. Johansson, I. Mäger, Y. Lee, K.E.M. Blomberg, M. Sadik, A. Alaarg, C.I.E. Smith, J. Lehtiö, S. EL Andaloussi, M.J.A. Wood, P. Vader, Cells release subpopulations of exosomes with distinct molecular and biological properties, Sci. Rep. 6 (2016) 22519.
- [49] B.J. Tauro, D.W. Greening, R.A. Mathias, S. Mathivanan, H. Ji, R.J. Simpson, Two distinct populations of exosomes are released from LIM1863 colon carcinoma cellderived organoids, Mol. Cell. Proteom. 12 (2013) 587–598.
- [50] B.E. Bouma, S.-H. Yun, B.J. Vakoc, M.J. Suter, G.J. Tearney, Fourier-domain optical coherence tomography: recent advances toward clinical utility, Curr. Opin. Biotechnol. 20 (2009) 111–118.
- [51] G.J. Tearney, M.E. Brezinski, B.E. Bouma, S.A. Boppart, C. Pitris, J.F. Southern, J.G. Fujimoto, In vivo endoscopic optical biopsy with optical coherence tomography, Science 276 (1997) 2037–2039.
- [52] M. Wojtkowski, High-speed optical coherence tomography: basics and applications, Appl. Opt. 49 (2010) D30.